Accuracy of the Spatial Representation of the Seafloor with Bathymetric Sidescan Sonars

PIERRE CERVENKA[1], UTE CHRISTINA HERZFELD[2] and CHRISTIAN DE MOUSTIER[3]

Marine Physical Laboratory, Scripps Institution of Oceanography, University of California, San Diego, 9500 Gilman Drive, La Jolla, CA 92093-0205, USA

[1] *Now at Laboratoire de Mécanique Physique, Université Paris VI, 78210 Saint-Cyr-l'Ecole, France*

[2] *Now at Institute of Arctic and Alpine Research, Boulder, Colorado 80309-0450, U.S.A.*

[3] *On leave at the Naval Research Laboratory, Code 7420, Washington D.C. 20375-5350, U.S.A.*

(Received 22 October 1992; in final form 30 June 1993)

Key words: Sidescan sonar, target location, bathymetry.

Abstract. When isobath maps of the seafloor are constructed with a bathymetric sidescan sonar system the position of each sounding is derived from estimates of range and elevation. The location of each pixel forming the acoustic backscatter image is calculated from the same estimates. The accuracy of the resulting maps depends on the acoustic array geometry, on the performances of the acoustic signal processing, and on knowledge of other parameters including: the platform's navigation, the sonar transducer's attitude, and the sound rays' trajectory between the sonar and the seafloor. The relative importance of these factors in the estimation of target location is assesed. The effects of the platform motions (e.g. roll, pitch, yaw, sway, surge and heave) and of the uncertainties in the elevation angle measurements are analyzed in detail. The variances associated with the representation (orientation and depth) of a plane, rectangular patch of the seafloor are evaluated, depending on the geometry of the patch. The inverse problem is addressed. Its solution gives the lateral dimensions of the spatial filter that must be applied to the bathymetric data to obtain specified accuracies of the slopes and depths. The uncertainty in the estimate of elevation angle, mostly due to the acoustic noise, is found to bring the main error contribution in across-track slope estimates. It can also be critical for along-track slope estimates, overshadowing error contributions due to the platform's attitude. Numerical examples are presented.

Introduction

Sound waves are used to map and image the seafloor because of their radiative properties in water. Such remote sensing operations are usually performed with side-looking sonar systems, or with multibeam echo-sounders [1]. Either class of sonar systems can be used to provide bathymetry and sidescanned imagery of the seafloor [2].

In this paper, we investigate the theoretical accuracy and resolution of the spatial representation of the seafloor when derived by a bathymetric sidescan sonar system. In such systems, the location of reflectors on the seafloor is derived from dynamic differential phase measurements of echoes received at the transducer rows. The phase differences are converted to elevation angles as a function of time [3], yielding depths and horizontal distances across-track. The magnitude and probable cause of uncertainties in the phase measurements have been reported elsewhere [4–5]. Here we are concerned with the resulting errors in locating targets. In addition to elevation angle errors, we take into account the sonar geometry, the location of the platform and its attitude at times of transmission and reception. Refraction effects provide additional range and angle errors that have been analyzed elsewhere [6]. Here, straight ray paths are assumed without loss of generality as this correction can be applied independently of the present study.

For sidescanned acoustic images of the seafloor, methods have been deviseds to correct pixel position for certain effects of varying platform attitude [7]. Here, we are interested in the qualitative and quantitative assessment of the image distortions. The classical flat bottom assumption is not used. Instead, backscatter values are mapped consistently with the co-registered bathymetric data.

Based on a few non-restrictive hypotheses, a set of equations is derived that serve two purposes: 1) assuming an exact, deterministic knowledge of the attitude parameters, the target location is calculated; 2) the effect of the sonar's attitude on the accuracy of the target's location is analyzed; and 3) from these

Marine Geophysical Researches **16**: 407–425, 1994.

error estimates, an assessment of the quality of the resulting seafloor mapping is made, giving practical indications on relevant data processing.

In Section 1, the geometry of the problem and the location of a target are formulated in terms of solutions derived up to the second order. Section 2 contains an error analysis applied to these formulae for each of the potential error sources. In Section 3, the analysis is expanded from the description of a single target's location to the statistical representation of a plane rectangular area of unknown orientation. Using additional hypotheses, the inverse problem is solved, providing a recipe for computing the theoretical resolution of a bathymetric sidescan sonar system. Numerical examples are given using realistic parameters that apply to the SeaMARC II system. To keep the text more readable, most of the derivations are given in the Appendices.

Notations

Most notations used in this text are summarized below, with the exception of variables only defined for intermediate steps. For the sake of clarity, the variables are introduced again when first encountered in the text.

The standard deviation of a variable, x, is denoted by the same letter as the variable, but with a tilde ($\tilde{x}$).

Platform:

- $P(l, m, m)$ location of the platform at transmit
- $Q(u, v, w)$ location of the platform at receive
- J mid-point of segment PQ
- i, j, k translation of the platform between transmit and receive ($\overrightarrow{PQ}$)
- $\alpha_T, \alpha_R, \alpha$ yaw at transmit, at receive, and averaged
- β_T, β_R, β pitch at transmit, at receive, and averaged
- μ roll at receive
- $\tilde{\gamma}$ approximate common value of $\tilde{\alpha}$, $\tilde{\beta}$ and $\tilde{\mu}$, when applicable

($\tilde{\alpha}, \tilde{\beta}, \tilde{\mu}$ refer to variations between pings)

Target:

- $2s$ round-trip slant range of a target
- τ measured time delay between ping transmission and echo reception
- ϕ measured elevation angle (relative to the fish's attitude)
- ξ error in the measured elevation angle
- $\psi = \phi + \mu + \xi$

Plane patch on the seafloor:

Geometry

- x_0, y_0, z_0 location of the center (relative to the platform's location)
- ρ_x, ρ_y along- and across-track dimensions
- θ_x, θ_y along- and across-track slopes

Sampling

- Δx along-track step between pings
- Δy across-track sampling (bathymetry)

Estimates

- ζ_x, ζ_y estimates of the slopes θ_x and θ_y
- h estimate of the fish's altitude above the center of the patch (z_0)

1. Target Location

1.1. Geometry of the problem

A reference frame in which the various attitude components are defined is provided in Figure 1. The cartesian coordinate system is oriented so that $\vec{x}$ represents the direction of travel, $\vec{y}$ the athwartship axis, and $\vec{z}$ the depth.

Depending on the application, all the parameters introduced below are assumed to be deterministic (their values are known perfectly) unless confidence limits are available to constrain their estimates. In the limit, parameters are set to zero to establish a reference estimate.

Let $P(l, m, n)$ denote the location of the fish at transmit time, and $Q_\tau(u, v, w)$ its position when receiving an echo at some time, τ, after transmission. P is unique for each ping, but Q_τ is an instantaneous location that varies with time as the echo signals are received. Consequently, a vector $\overrightarrow{PQ}$ is associated with each instantaneous return, and its components i, j, k represent respectively the principal forward translation of the fish occasionally altered by surge, the lateral shift (sway) potentially incurred by drift or yaw, and the vertical component due to heave or pitch.

$$\overrightarrow{PQ} = (i = u - l, j = v - m, k = w - n). \quad (1)$$

It is also convenient to define J as the midpoint of segment PQ:

$$\overrightarrow{PJ} = \overrightarrow{JQ} = \overrightarrow{PQ}/2. \quad (2)$$

The rotation angles are defined as follows: Roll is a rotation about the fore-aft axis of the array, pitch is the vertical angle between this axis and the horizontal plane, and yaw is the horizontal angular deviation of this axis from the mean course of the fish.

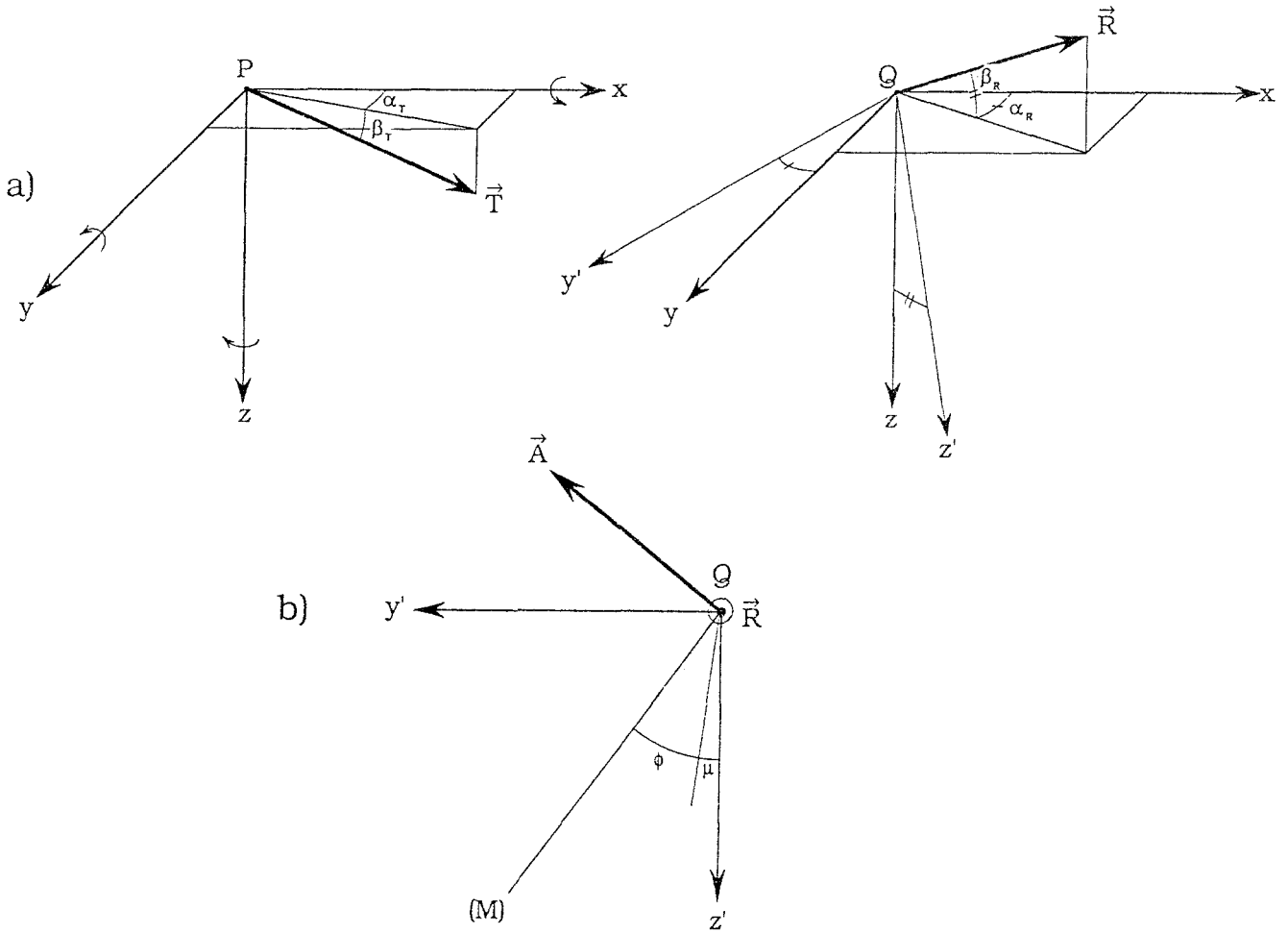

Fig 1. Geometry of the problem. (a) Fish at transmit and receive, (b) Elevation angle measurement. Note that in this figure α_T, α_R, and β_R are positive, whereas β_T, ϕ, μ, and $\psi = \phi + \mu$ are negative.

Orientations of these angles are described in Figure 1. At transmit time (point P), we are only concerned with yaw (α_T) and pitch (β_T). Roll at transmit is not a factor in the estimation of the target location, it only affects the magnitude of the return due to the rotation of the broad athwartship beam pattern (typically $> 70°$ wide at the half power points). However, roll is critical on receive as it is directly linked to the elevation angle estimation. Yaw (α_R), pitch (β_R) and roll (μ) are therefore used on receive (Q).

Using these rotation angles, the orientation of the main axis of the transducer rows is represented by the unit vectors $\vec{T}$ at P and $\vec{R}$ at Q:

$$\vec{T} = M_z(\alpha_T)M_y(\beta_T)\begin{bmatrix}1\\0\\0\end{bmatrix} = \begin{bmatrix}\cos\beta_T \cos\alpha_T\\ \cos\beta_T \sin\alpha_T\\ -\sin\beta_T\end{bmatrix} \quad (3)$$

$$\vec{R} = M_z(\alpha_R)M_y(\beta_R)\begin{bmatrix}1\\0\\0\end{bmatrix} = \begin{bmatrix}\cos\beta_R \cos\alpha_R\\ \cos\beta_R \sin\alpha_R\\ -\sin\beta_R\end{bmatrix} \quad (4)$$

where the rotation matrices $M_y(\beta)$ and $M_z(\alpha)$, respectively describing pitch and yaw, are expressed in Eq. (B3) in the appendices.

The main steps necessary to obtain the results are presented below. However, for a complete mathematical derivation, the hypotheses and intermediate steps referenced in the main text are given in the Appendix.

Assuming that the echo received at Q comes from an ideal point scatterer on the seafloor, $M(x, y, z)$, the range and angle estimation problem is predicated on the conditions listed below (the relevant hypotheses are summarized in Appendix A).

(1) The elevation angle ψ is derived from the angle of arrival, ϕ, measured at Q in the plane normal to $\vec{R}$ (Figure 1b), with some error, ξ, while the fish has rolled an angle μ:

$$\psi = \phi + \mu + \xi. \tag{5}$$

Hence, the target M belongs to the plane $(Q, \vec{A})$ obtained after rotating a vertical plane around $\vec{R}$ with an angle ψ:

$$\overrightarrow{QM} \cdot \vec{A} = 0 \tag{6}$$

(Appendix B-I).

(2) The roundtrip range to M, $2s$, is derived from the measured time delay, τ, and a sound velocity, c, integrated over the water column:

$$2s = |\overrightarrow{PM}| + |\overrightarrow{MQ}| = c\tau. \tag{7}$$

This equation implies that for a fixed value of s, the locus of point M is an ellipsoid with focus points P and Q, and major axis $2s$. Its eccentricity is close to unity as the distance PQ traveled between transmit and receive is much smaller than the range to the target, JM or s (Hypothesis I in Appendix A). Therefore, the athwartship sector of this surface is approximated by the inner tangent sphere of equation:

$$JM^2 = s^2 - (PQ/2)^2, \tag{8}$$

which is exact up to the third order (Appendix B-II).

(3) The point M belongs to the domain of maximal insonification defined by the product of transmit and receive beam directivities. With a sidescan sonar system, both beam patterns are usually identical. The sonar platforms are designed to be stable enough for the transmit and receive beams to overlap properly (Hypothesis II in Appendix A) so that the farfield crossproduct area of maximal insonification can be approximated by the median plane, (Π_M) (Figure 2):

$$(\vec{R} + \vec{T}) \cdot \overrightarrow{JM} \approx 0 \tag{9}$$

(Appendix B-III).

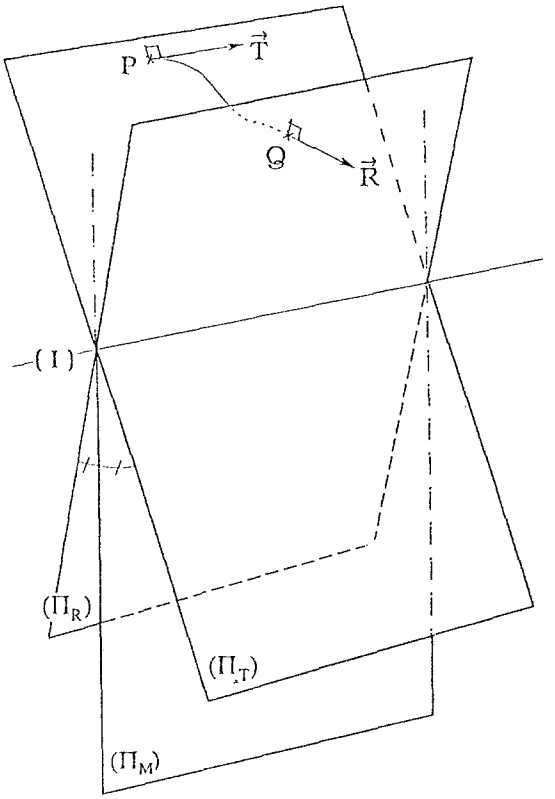

Fig. 2. Farfield maxima of acoustic beam patterns
(Π_T): at transmit ($\vec{T} \perp \Pi_T$):
(Π_R): at receive ($\vec{R} \perp \Pi_R$);
(Π_M): beam pattern product.

1.2. Solutions

Second Order Solution

The location of the target M can be found by solving the set of simplified Eqs. (6, 8, 9), which amounts to finding the intersection of two planes and a sphere. Calculations are carried to the second order and are detailed in Appendix B-IV. For the sake of clarity, terms involving elevation, ψ, are often kept in the trigonometric form, although it must be remembered that $\cos\psi$ and $\sin\psi$ stand respectively for:

$$\cos\psi = \cos\phi - (\mu + \xi)\sin\phi - \tfrac{1}{2}(\mu + \xi)^2\cos\phi, \tag{10}$$

and

$$\sin\psi = \sin\phi + (\mu + \xi)\cos\phi - \tfrac{1}{2}(\mu + \xi)^2\sin\phi. \tag{11}$$

The x, y, z coordinates of M are then given by:

$$x = l + \tfrac{1}{2}i + s(\beta\cos\phi + \alpha\sin\phi), \tag{12}$$

(first order relation)

$$y = m - s\sin\psi + j\frac{1+\cos^2\phi}{2} + s\alpha\left(\beta\cos\phi + \alpha\frac{\sin\phi}{2}\right) + \frac{\cos\phi}{2}[i(\beta\sin\phi - \alpha\cos\phi) + k\sin\phi], \quad (13)$$

$$z = n + s\cos\psi + k\frac{1+\sin^2\phi}{2} - s\beta^2\frac{\cos\phi}{2} + \frac{\sin\phi}{2}[i(\beta\sin\phi - \alpha\cos\phi) + j\cos\phi], \quad (14)$$

where α and β denote respectively, the average yaw and pitch:

$$\alpha = \frac{\alpha_T + \alpha_R}{2} \quad \text{and} \quad \beta = \frac{\beta_T + \beta_R}{2}. \quad (15)$$

In Eqs. (12–14), terms are displayed in increasing order from left to right. First order terms include i, and any products of s with α, β, μ, or ξ. Second order terms are j, k, and products such as $(\alpha, \beta, \mu, \xi)i$ or $(\alpha^2, \alpha\beta)s$.

No Drift

The second order results of Eqs. (12–14) are simplified further if one assumes that there is no drift. This condition entails that the platform's heading is always tangent to the trajectory. Recalling the assumption that attitude angles vary slowly in the time frame of the signal reception, it follows that j and k are related to i through the average angles α and b (Eq. 15) according to:

$$j = \alpha i \quad \text{and} \quad k = -\beta i. \quad (16)$$

As a result, the number of independent variables that must be taken into account in the set (i, j, k, α, β), is reduced from five to three. Eq. (12) remains unchanged but Eqs. (13–14) are further simplifed, so that the coordinates of point M are now given by:

$$x = l + \tfrac{1}{2}i + s(\beta\cos\phi + \alpha\sin\phi), \quad (17)$$

$$y = m - s\sin\psi + \tfrac{1}{2}j + s\alpha\left[\beta\cos\phi + \alpha\frac{\sin\phi}{2}\right], \quad (18)$$

$$z = n + s\cos\psi + \tfrac{1}{2}k + s\beta^2\frac{\cos\phi}{2}. \quad (19)$$

Although more than three parameters appear in these three equations, they are written consistently as no more than three independent parameters are used in each of them.

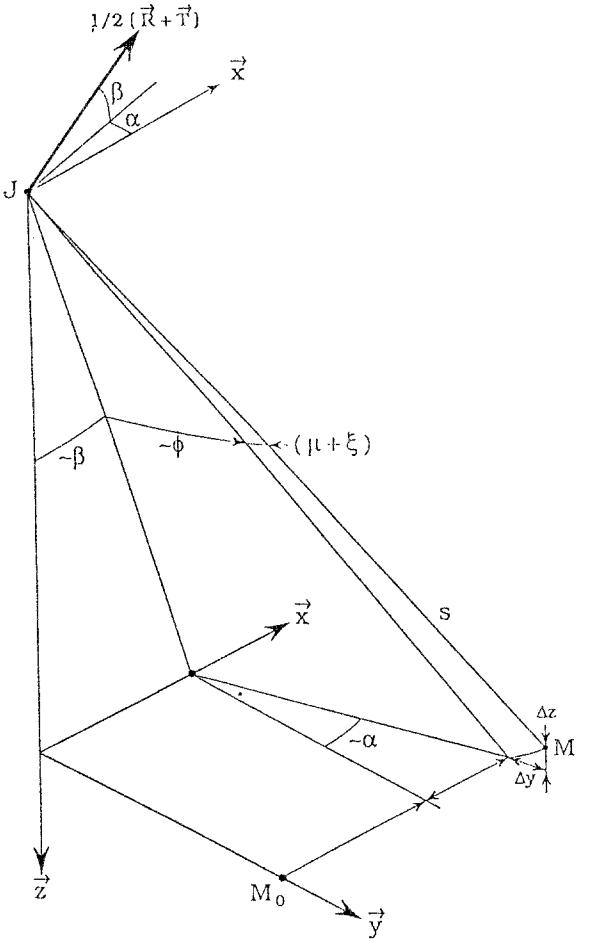

Fig. 3. Approximate location of the target M with respect to attitude angles α, β, μ, elevation angle ϕ, and error in the elevation measurement ξ. M_0 is the "zero-order" location. Considering the angle orientations defined in Figure 1, α and ϕ are negative in this figure.

First Order Solution

Finally, the first order solution with or without drift is given by:

$$x = x_0 + \tfrac{1}{2}i + s(\beta\cos\phi + \alpha\sin\phi), \quad (20)$$

$$y = y_0 - s(\mu + \xi)\cos\phi, \quad (21)$$

$$z = z_0 - s(\mu + \xi)\sin\phi, \quad (22)$$

with the zero order components:

$$x_0 = l,\ y_0 = m - s\sin\phi,\ z_0 = n + s\cos\phi. \quad (23)$$

The geometrical interpretation of these equations is quite intuitive, as shown on Figure 3.

In most applications, the zero order set of Eq. (23) is used, under the basic assumptions made when mapping bathymetric or acoustic backscatter amplitude data: (1) attitude variations are negligible ($\vec{T} = \vec{R} = \vec{x}, \mu = 0$), (2) the translation of the sonar between transmission and reception is ig-

nored ($P = Q$), and (3) the elevation angle is known exactly ($\xi = 0$).

2. Error Analysis

When all the parameters are known exactly, the center of the beam footprint is found through one of the set of Eqs. (12–14), (17–19), (20–22) or (23), depending on the level of approximation specified. When an uncertainty is associated with these parameters, the same equations can be used straightforwardly to derive the resulting errors on x, y, and z, as long as the error on any parameter remains consistent with the initial assumptions (e.g. δi is a first order length).

In this Section, the effects of errors associated with each parameter are analyzed in detail. To this end, and without any loss of generality, it is convenient to define δM as the error on the target location given by Eq. (23).

2.1. Effects of slant range errors

The slant range, s, is derived from the product of a time delay, τ, by an average sound velocity, c (Eq. 7), so the accuracy with which these two values are known dictates the accuracy on s. The average sound velocity c is calculated by integrating local values over the water column, and the accuracy of this process is usually better than a few percents. Uncertainties associated with the time delay are dictated by the auto-correlation length of the transmitted pulse, which is usually much smaller than the time delay itself (a ratio of 1/1000 is typical).

The error associated with terms involving slant range is an order of magnitude less than the order of the terms themselves. Hence, to evaluate inaccuracies in the target location due to δs, it is sufficient to consider terms of the zeroth order for δx and terms up to the first order for δy and δz. Also, because x_0 is independent of s (Eq. 23), errors in slant range have no effect on the along-track mapping. Likewise, the first order expressions of y (Eq. 21) and z (Eq. 22) are linear is s, so that slant range errors are directly reported in the $(\vec{y}, \vec{z})$ plane (Figure 4). However, the relative error $\delta s/s$ is likely to be fairly systematic over a given homogeneous portion of survey. As a consequence, slant range errors will typically introduce the same amount of across-track scale error in backscatter images and bathymetry mapping, and a multiplicative distortion in the same proportion will also affect the bathymetric data.

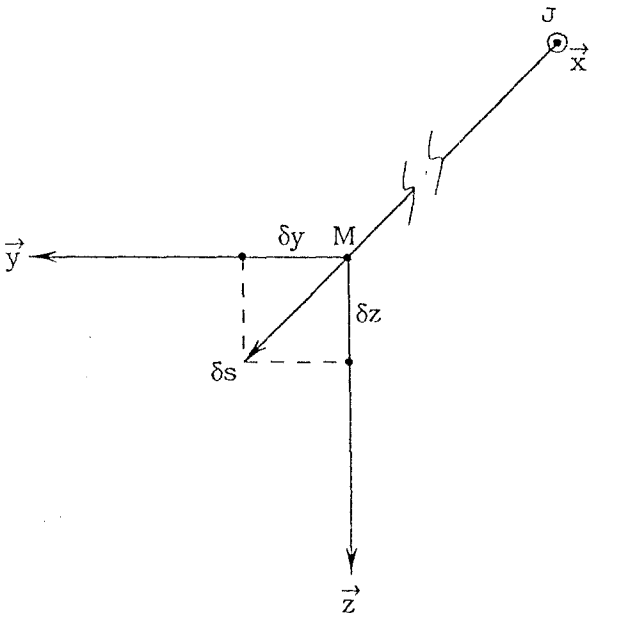

Fig. 4. As the reflector M lies in a plane which is quasi perpendicular to $\vec{x}$, the error in slant range δs is directly reported in the $(\vec{y}, \vec{z})$ plane.

The error in position relative to the position of the fish at transmit can then be summarized by:

$$\delta_s x = 0, \quad \text{and} \quad \frac{\delta_s y}{y - m} = \frac{\delta_s z}{z - n} = \frac{\delta s}{s} \qquad (24)$$

$$\text{with} \quad \frac{\delta s}{s} = \frac{\delta c}{c} + \frac{\delta \tau}{\tau}.$$

2.2. Effects of errors in sonar location

Errors associated with sonar location involve the fish's position (P) at the instant of transmission, and its translation to the instantaneous reception points (Q_τ). Without loss of generality, it can be assumed that the reference point, O, is the estimated location of P so that $\overrightarrow{OP}$ represents the error in position at transmission time:

$$\overrightarrow{\delta_P M} = \overrightarrow{OP} \quad \text{i.e.} \quad \delta_P(x, y, z) = (l, m, n). \qquad (25)$$

Terms related to the translation of the fish in Eqs. (13–14) indicate that the second order approximations of y and z are linear with respect to i, j and k, so that it is possible to use this set of general equations to derive directly:

$$\delta_{PQ} x = \tfrac{1}{2}\delta i, \qquad (26)$$

$$\delta_{PQ}y = \frac{1+\cos^2\phi}{2}\delta j + \frac{\cos\phi}{2}[\delta i(\beta\sin\phi - \alpha\cos\phi) + \delta k\sin\phi], \quad (27)$$

$$\delta_{PQ}z = \frac{1+\sin^2\phi}{2}\delta k + \frac{\sin\phi}{2}[\delta i(\beta\sin\phi - \alpha\cos\phi) + \delta j\cos\phi]. \quad (28)$$

When there is no drift (Eq. 16), Eqs. (17–19) give the very simple result:

$$\delta_{PQ}(x, y, z) = \tfrac{1}{2}(\delta i, \delta j, \delta k) \text{ i.e. } \delta_{PQ}\overrightarrow{M}\ \overrightarrow{PQ}/2. \quad (29)$$

This error includes two parts: the forward motion of the fish (in essence, δi); and small fluctuations (sway, heave and surge) typical for a towed instrument (respectively, δj, δk and a second order part of δi). The overall target position error due to uncertainties in the fish's location is obtained by combining Eqs. (25) and (29), yielding the vector $\overrightarrow{OJ}$ such that:

$$\delta_{P,Q}\overrightarrow{M} = \overrightarrow{OP} + \overrightarrow{PQ}/2 = \overrightarrow{OJ}. \quad (30)$$

If the estimated fish track departs from its actual trajectory, the difference is directly embedded in the resulting maps. The first contribution (Eq. 25) is linked to the navigation and the difficulty of estimating the fish's position relative to the towing vessel. It reflects slowly changing large offsets, compared to the small but faster variations recorded in the second order part of Eq. (29). The main contribution of this equation reflects the global distortion of the backscatter images or of the bathymetry which occurs in the along-track direction whenever the fish's translation is not taken into account.

A seemingly paradoxical result appears in Eqs. (29–30): heave has no effect on the athwartship mapping ($\delta_k y = 0$). Two observtions can be made: 1) This result is derived by assuming that the instantaneous direction of the fish remains tangent to its trajectory. Compared with Eq. (27), here the pitch angle that generates a vertical displacement compensates exactly the lateral deviation (δy) that would otherwise occur. 2) The offset $n = OP_z$ biases the bathymetry through the error on the fish's tow depth. However, in the formalism presented here, the backscatter mapping is based on the assumed altitude of the fish, which is independent from this bias. By comparison, such an offset has a dramatic influence on pixel location when the backscatter mapping is based on a flat bottom assumption, or on an independent bathymetry data base. As a consequence, a backscatter image whose pixel location is directly processed through the whole set of information collected by the bathymetric sidescan sonar system is likely to be more accurate than using any other pixel relocation scheme.

2.3. Effects of uncertainties in roll, pitch, yaw, and elevation

In the set of Eqs. (12–14), elevation perturbations $(\mu+\xi)$ have no effect on x but affect first order terms in y and z (through Eqs. 10–11). Hence, roll and elevation measurements are the leading causes of error on $(y-m)$ and $(z-n)$.

$$\delta_\phi x = 0, \quad (31)$$

$$\delta_\phi y = -s\cos\phi\delta\phi, \quad (32)$$

$$\delta_\phi z = -s\sin\phi\delta\phi,$$

with

$$\delta\phi = \delta\mu + \delta\xi. \quad (34)$$

Conversely, there is no first order error due to pitch or yaw on y and z, whereas for the along-track component x, the error is given by:

$$\delta_{\alpha,\beta}x = s\sin\phi\delta\alpha + s\cos\phi\delta\beta. \quad (35)$$

Compared to the zero-order mapping of a single ping (Eq. 23), the distortions introduced by these angles are clearly viewed by noticing that Eqs. (32–35) yield the following approximations:

$$\delta x \approx (z-n)\delta\beta - (y-m)\delta\alpha, \quad (36)$$

$$\delta y \approx -(z-n)(\delta\mu + \delta\xi), \quad (37)$$

$$\delta z \approx (y-m)(\delta\mu + \delta\xi). \quad (38)$$

The first two equations describe how the attitude of the platform affects the mapping of backscatter data or bathymetry data, whereas Eq. (38) concerns only the latter. As mentioned at the end of Section 1.2, in a system such as SeaMARC II, data are mapped without taking into account the variations of the attitude angles during a ping cycle. The errors $\delta\alpha$, $\delta\beta$, and $\delta\mu$ take the values of the attitude angles themselves. In addition, the errors are highly correlated for contiguous samples within the same ping because the sampling interval is much shorter than the time scale of the dynamics of the vehicle motion. If the attitude parameters change sufficiently slowly, on a time scale commensurate with the

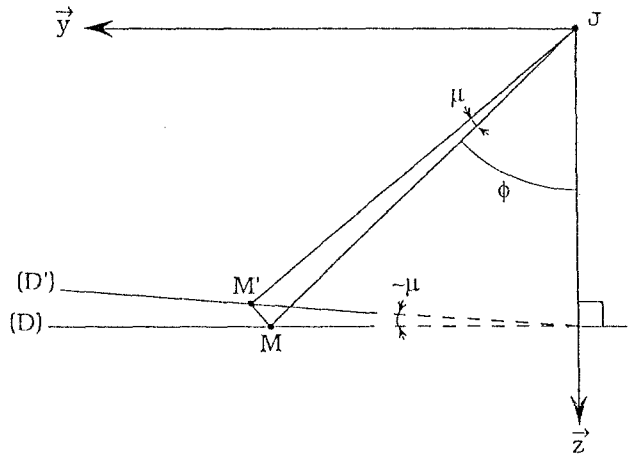

Fig. 5. For a horizontal bottom profile (D), each point M is transformed into M' by rotation around $\vec{x}$ with the small angle μ. For points such that the angle ϕ is not too small, the locus of M' can be approximated by the straight line (D') which forms an angle μ with (D).

duration of echo reception from the seafloor for a given ping, in the limit the attitude variations can be considered negligible so that the corresponding errors change only from one ping to the next.

Looking at this idealized figure for a single raster line, Eq. (35) shows that the along-track shifts result from two effects that can be interpreted as (Figure 3): 1) A forward or backward shift caused by pitch, whose cross-track variations are dictated by the corresponding bathymetric profile. Within a homogeneous portion of survey, this translation can be approximated as an along-track offset. As the along-track width of the footprint of the beam pattern increases across-track from nadir out, the relative effect of pitch prevails near nadir. 2) Yaw causes a global rotation of each raster line, independent of the relief. Hence, unlike pitch, the effect of yaw is negligible in the central part of the swath.

Both Eqs. (37–38) are a sum of two terms whose effects differ because of their behavior between adjacent samples. In the case of roll, if we consider a segment of raster line whose time span is significantly shorter than the roll period, Eq. (37) implies that roll contributes to the global lateral translation of this segment of bathymetric profile or sidescan raster line when the variance of the profile is not too large. Accordingly, Eq. (38) implies that roll introduces a bias in the bathymetry, independent of the local relief, by adding a cross-track slope μ (Figure 5). Depending on the extent of the roll period, the validity of the approximation may be questionable over a whole raster line. However, the analysis developed in Section 3 concerns rectangular patches of the seafloor whose width is only a fraction of the total swath width, so that the above approximation applies.

Conversely, the error $\delta\xi$ can be considered as random, without any coherence from one elevation measurement to another. The magnitude of this error is mostly dictated by the signal-to-noise ratio of the seafloor echoes. For each side, bathymetric samples are derived within an athwartship sector approximately bound in elevation between 10°–15° and 55°–60°. The lower limit is meant to eliminate the near-nadir specular reflections that cannot provide useful phase measurements. The upper limit corresponds to the onset of the first bottom multiple echo which is often strong enough to cause dramatic interference in the phase measurement. Hence, within this sector, the relative variations of slant range remain smaller than 2. In addition, the arrays are mounted on the platform with a tilt angle (e.g. about 45° for SeaMARC II) so that the directivity in the across-track plane compensates partially for the slant range variations. Consequently, the deviation of the elevation error, ξ, can be approximated by a constant when considering a set of bathymetric samples gathered over a homogeneous area. This approximation is in agreement with the variances that are observed when processing raw data recorded with the SeaMARC II system [4]. It also applies to the small rectangular patches of seafloor that are considered in Section 3.

2.4. Spatial sampling

Regardless of the accuracy of the measurements, the quality of the seafloor representation derived from data collected with a bathymetric sidescan sonar system depends also on the spatial sampling process. This process is usually anisotropic. Due to the finite acoustic beamwidth (θ_{3dB}) in the along-track dimension, and the short horizontal projection of the pulse length in the cross-track dimension (dy), each seafloor echo received results from the signals backscattered by a narrow strip of length dx along-track. Considering a homogeneous portion of survey for which the average altitude of the fish is denoted $h = z - n$, the length of the footprint is simply estimated by:

$$dx \approx s\theta_{3dB} \approx (h^2 + y^2)^{1/2}\theta_{3dB}. \qquad (39)$$

This echo integration over each strip reduces the apparent spatial bandwidth of the along-track relief

to the approximate spatial frequency:

$$\nu_{\max} \approx (2dx)^{-1}. \tag{40}$$

Hence, the speed of the ship and the transmission period are adjusted according to the aperture of the transducer array (θ_{3dB}) and the average altitude of the fish above the surveyed area (h), so as to provide an along-track step Δx with minimal spatial aliasing:

$$dx \geq \Delta x \qquad (\geq i). \tag{41}$$

It is important to note that the along-track resolution is bound by the spatial frequency $\nu_{\max}$ given in Eq. (40), which may be much lower than the optimistic value $(2\Delta x)^{-1}$.

The cross-track sampling of the backscatter data is approximated by dy. However, bathymetry data usually require longer spatial integration intervals across-track (Δy). A lower limit on this interval is dictated by the angular resolution, ξ, of the elevation measurements:

$$\Delta y \approx h\xi. \tag{42}$$

This interval also implies that the data will only contain components of the relief with cross-track spatial frequency up to $(2\Delta y)^{-1}$.

3. Representation of a Plane, Rectangular Area

3.1. Theoretical development

As indicated in Section 2, the uncertainty associated with the sonar's attitude and position during measurements has a direct impact on bathymetric accuracy and on proper positioning of backscatter pixels. In this section, the analysis is expanded from errors in the location of a single target to a theoretical assessment of the sonar system's ability to reproduce faithfully the spatial characteristics of the terrain surveyed. One way to approach this problem is to determine the size of a patch of seafloor whose depth and slopes can be properly represented with the system.

The analysis is restricted to small-scale fluctuations. Systematic distortions due to slant range errors and the along-track progression of the fish are not addressed here. Variations occurring very slowly from one ping to another due to navigation errors, as well as the remaining second order fluctuations in the position of the fish, are also neglected. Consequently, only first order effects of uncertainties in roll, pitch, yaw, and elevation are considered, through Eqs. (36–38). The analysis builds on the first order approximations derived in Section 1.2, but i is discarded in Eq. (20), and the origin of coordinate O is reset, for convenience, at the initial fish position P ($l = m = n = 0$) in Eqs. (20–23).

We consider a sloping, rectangular, plane area centered at point $H(x_0, y_0, x_0)$ whose equation is:

$$\overrightarrow{HM} \cdot \vec{N} = 0 \tag{43}$$

with

$$\vec{N} = (\sin\theta_x \cos\theta_y, \; -\sin\theta_y \cos\theta_x, \cos\theta_x \cos\theta_y),$$

where θ_x and θ_y respectively stand for along- and across-track slopes. We assume that this patch has been surveyed with $(2L + 1)$ pings consisting of $(2W + 1)$ across-track samples each. Within this patch of seafloor, $z_{p,q}$ denotes the depth of the qth across-track bathymetric sample from the pth ping, deduced from measurements of pairs $(\phi, s)_{p,q}$, i.e. $z_{p,q} = s_{p,q} \cos\phi_{p,q}$. The representation of the relief is built with points $(x_p, y_q, z_{p,q})$, by mapping the assumed depth values $z_{p,q}$ at the theoretical locations (x_p, y_q) in the horizontal plane:

$$x_p = x_0 + p\Delta x \qquad (-L \leq p \leq L), \tag{44}$$

$$y_q = y_0 + q\Delta y \qquad (-W \leq q \leq W). \tag{45}$$

However, due to the fish movements and the noise in the elevation measurements, the processed echoes come from actual locations on the seafloor centered at points $M(x_p + \delta x, y_q + \delta y, z_{p,q} + \delta z)$. Consequently, the mapped depth values are deduced by solving the plane Eq. (43) so that, using Eqs. (44–45), it gives:

$$\begin{aligned} z_{p,q} = z_0 &- (p\Delta x + \delta x)\tan\theta_x \\ &+ (q\Delta y + \delta y)\tan\theta_y - \delta z \end{aligned} \tag{46}$$

with the intervals δx, δy and δz as defined in Eqs. (36–38).

Given the set $\{z_{p,q}\}$ over the rectangular array, we are interested in the statistical characteristics of the representation of the seafloor, i.e. the estimates of the slopes (ζ_x and ζ_y) and of the depth h at the center of the patch, as well as their variances ($\tilde{\zeta}_x^2$, $\tilde{\zeta}_y^2$, and $\tilde{h}^2$). The uncertainty associated with each sample, M, is treated as noise made up of a combination of uncertainties in roll, pitch, yaw and elevation. However, the attitude variations are considered quasi static for the time interval during which seafloor echoes are received. Therefore, for ping number p, the attitude angles take the values

α_p, β_p and μ_p. As ξ accounts for the noise in the elevation measurement itself, it varies independently for each sample q within a ping: $\xi = \xi_{p,q}$. All these quantities are assumed to be Gaussian random variables with standard deviations $\tilde{\alpha}$, $\tilde{\beta}$, $\tilde{\mu}$ and $\tilde{\xi}$, respectively. As systematic distortions are not addressed here, they are assumed also to be zero mean.

A two-dimensional linear regression is performed on the set $\{z_{p,q}\}$ to provide the estimates ζ_x, ζ_y, and h. They are obtained by minimizing the mean square distance between the estimated plane and the samples:

$$\sum_p \sum_q D_{p,q}^2 \quad \text{minimal!}$$

with (47)

$$D_{p,q} = -p\Delta x \tan \zeta_x + q\Delta y \tan \zeta_y + h - z_{p,q}.$$

This classical least squares problem requires to solve:

$$\sum_p \sum_q D_{p,q} = 0, \sum_p \sum_q D_{p,q} p = 0, \sum_p \sum_q D_{p,q} q = 0. \quad (48)$$

Using the resultant estimates, the corresponding variances are calculated. Owing to the Gaussian statistics assumption, the calculations are carried out using linearity of the variance for independent variables. Details are found in Appendix C, with explicit results in Eqs. (C12, C14–C15). However, much simpler results can be obtained if the following additional conditions, owing to the specific situation of sidescan sonar systems, are considered:

Condition 1: Qualifying the ability of a bathymetric sidescan sonar system to give a meaningful representation of the seafloor requires that the size of the test patches (ρ_x along-track by ρ_y across-track) remains reasonable compared to the whole geometry of the setup. In other words, we are only interested in finding statistics over area limited to:

$$\rho_x = (2L + 1)\Delta x \lesssim z_0.$$

and (49)

$$\rho_y = (2W + 1)\Delta y \lesssim z_0.$$

Condition 2: As implied by the current capabilities of shallow-towed bathymetric side-looking sonar systems, valid bathymetric samples are obtained on each side over relatively narrow athwartships angular sectors (e.g. usually smaller than the interval]10°–60°[). Hence, no restrictions are imposed when considering small rectangular patches of the mapped seafloor such that the coordinates of their center, y_0 and z_0, have the same order of magnitude. In addition, the technique based on differential phase measurements is not appropriate for deriving bathymetric samples from specular echoes. Therefore the analysis applies only to seafloor patches whose orientation does not yield specular returns.

Condition 3: This study is limited to seafloors yielding bathymetries without very steep slopes: Doing so, the tangents of these slopes cannot be much larger than unity. There are several reasons why this restriction will not inhibit the generality of the results: First, this condition is consistent with Condition 2 ($z_0 \approx y_0$) for the across-track slopes, if one notices that a sidescan sonar cannot properly map areas that either lie in an acoustic shadow ($y_0 \tan \theta_y \geq z_0$) or generate multiple synchronous echoes ($z_0 \tan \theta_y \leq -y_0$). In addition, the spatial sampling inherent to the sonar system (Section 2–4) has the effect of smoothing the representation of the relief. Another smoothing effect occurs because of the size of the rectangular patches used in the least squares fitting processes applied to build the bathymetry.

Condition 4: Generally, amplitudes of the fish angular movements are similar in every direction, i.e. $\tilde{\alpha}$ and $\tilde{\beta}$ have the same order of magnitude. In addition, we assume in this paper that roll ($\tilde{\mu}$) has also the same order of magnitude. However, there is no such relation for the noise in the measurements of the elevation angle ($\tilde{\xi}$), whose average amplitude is usually larger than the angular variations in attitude.

The solutions under these conditions are given in Appendix C (Eqs. C16–C18). Several particular cases of interest can be derived.

Single datum

The variance of a single bathymetric datum can be directly calculated from Eq. (C18) with $L = W = 0$:

$$\tilde{h}^2 = (\tilde{\alpha}^2 y_0^2 + \tilde{\beta}^2 z_0^2)\tan^2 \theta_x + (\tilde{\mu}^2 + \tilde{\xi}^2)(y_0 + z_0 \tan \theta_y)^2. \quad (50)$$

Following the restriction introduced by Condition 2, the validity of the contribution of elevation uncertainties ($\tilde{\mu}$ and $\tilde{\xi}$) is limited to seafloor patches that do not yield specular reflections, i.e. such that the term $(y_0 + z_0 \tan \theta_y)$ is not very small when θ_x is very small. This restriction applies also for the results that follow.

Now, looking at single lines or rectangular areas, further simplifications apply when there are at least 5 samples ($N \geq 2$) along the given direction, as the

ratio $(N+1/2)^2N^{-1}(N+1)^{-1}$ is then very close to unity. Eqs. (C16–C18) give finally in the three following cases:

Part of a single ping

When $L=0$ the expected accuracy in mapping part of an across-track profile is given by:

$$\tilde{\zeta}_y^2 \approx (\tilde{\alpha}^2\cos^2\theta_y + \tilde{\beta}^2\sin^2\theta_{\tilde{y}})\tan^2\theta_x\cos^2\theta_y + \tilde{\mu}^2 + \tilde{\xi}^2\frac{12\Delta y}{\rho_y^3}(y_0\cos\theta_y + z_0\sin\theta_y)^2\cos^2\theta y, \tag{51}$$

$$\tilde{h}^2 \approx (\tilde{\alpha}^2 y_0^2 + \tilde{\beta}^2 z_0^2)\tan^2\theta_x + \left(\tilde{\mu}^2 + \tilde{\xi}^2\frac{\Delta y}{\rho_y}\right)(y_0 + z_0\tan\theta_y)^2. \tag{52}$$

Along-track segment

Likewise, when $W=0$, results for an along-track line are:

$$\tilde{\zeta}_x^2 \approx 12\cos^2\theta_x\frac{\Delta x}{\rho_x^3}[(\tilde{\alpha}^2 y_0^2 + \tilde{\beta}^2 z_0^2)\sin^2\theta_x + (\tilde{\mu} + \tilde{\xi}^2)(y_0 + z_0\tan\theta_y)^2\cos^2\theta_x], \tag{53}$$

$$\tilde{h}^2 \approx \frac{\Delta x}{\rho_x}[(\tilde{\alpha}^2 y_0^2 + \tilde{\beta}^2 z_0^2)\tan^2\theta_x + (\tilde{\mu}^2 + \tilde{\xi}^2)(y_0 + z_0\tan\theta_y)^2]. \tag{54}$$

Rectangular patch

Now, we report the case of a rectangular patch which is relevant to our initial question. The approximated variances over slopes are given by:

$$\tilde{\zeta}_x^2 \approx 12\cos^2\theta_x\frac{\Delta x}{\rho_x^3}\left[(\tilde{\alpha}^2 y_0^2 + \tilde{\beta}^2 z_0^2)\sin^2\theta_x + \left(\tilde{\mu}^2 + \tilde{\xi}_x\frac{\Delta y}{\rho_y}\right)(y_0 + z_0\tan\theta_y)^2\cos^2\theta_x\right], \tag{55}$$

$$\tilde{\zeta}_y^2 \approx \frac{\Delta x}{\rho_x}\left[(\tilde{\alpha}^2\cos^2\theta_y + \tilde{\beta}^2\sin^2\theta_y)\tan^2\theta_x\cos^2\theta_y + \tilde{\mu}^2 + \tilde{\xi}^2\frac{12\Delta y}{\rho_y^3}(y_0\cos\theta_y + z_0\sin\theta_y)^2\cos^2\theta_y\right], \tag{56}$$

whereas the standard deviation over the depth offset is simply related to that of the across-track slope's through:

$$\ddot{h} = \frac{0.3}{\cos^2\theta_x}\tilde{\zeta}_x\rho_x. \tag{57}$$

Anticipating on the results deduced later on in Appendix D (Eq. D7), we mention here that using realistic numerical figures, the influence of the attitude movements upon the across-track variance is very weak so that Eq. (56) can often be reduced to:

$$\tilde{\zeta}_y^2 \approx 12\cos^2\theta_y\frac{\Delta x\Delta y}{\rho_x\rho_y^3}(y_0\cos\theta_y + z_0\sin\theta_y)^2\tilde{\xi}^2. \tag{58}$$

Hence, for bathymetry built after filtering the data in both along- and across-track directions and according to the approximate result in Eq. (58), the accuracy on the across-track slopes is mostly dictated by the noise in the elevation angle measurements. On the other hand, all the angular variations (attitude and noise) contribute to the along-track slope error and the depth offset. A simple analysis of the previous results leads to the following comments:

Variance of the across-track slope (Eq. 58)

The effect of the noise in the elevation measurement is maximal for a small grazing angle, i.e. with $\theta_y = \frac{1}{2}\arctan(z_0/y_0)$. It vanishes for patches whose cross-track orientation tends to be perpendicular to the platform-target direction, i.e. for $\theta_y = -\arctan(y_0/z_0)$, except when θ_x is very small and leads to specular reflections.

The actual along-track slope has no influence on the across-track slope estimate. However, as mentioned previously, Eq. (58) is not valid in case of specular inflection, which may occur only if $|\theta_x|$ is very small (e.g. $< 5°$).

Variance of the along-track slope (Eq. 55)

The contributions of pitch and yaw are independent of the across-track slopes (θ_y) and increase with the along-track slope to be maximal at $|\theta_x| = 45°$.

The influences of roll and noise are divided by 4 when the along-track slope varies from 0° to 45°. However, the most dramatic changes occur with the across-track slope. When the seafloor patch yields specular returns, the influence of these parameters is vanishing (regardless of θ_x), whereas their contribution is maximal if the area is seen at a very small grazing angle.

Depth offset (Eq. 57)

The contributions of pitch and yaw are independent of the across-track slopes (θ_y) and increase with the along-track slopes.

The contributions of roll and noise are independent of the along-track slopes (θ_x). The behavior of

these two parameters with respect to the across-track slopes is the same as for the estimated along-track slope.

3.2. Inverse problem

The formulas derived above are useful in cases where the degree of confidence of the mapping results must be evaluated. The inverse problem is of more practical interest: it can be defined as finding the size of the window (ρ_x, ρ_y) that must be used to convolve the data in order to produce a smoothed bathymetry whose accuracy is quantified by a given variance, ζ^2, in the estimated slopes. As concluded from Eqs. (55–56), the variances in the slopes depend on many parameters, and typical lengths ρ_x and ρ_y must be estimated by using values that are representative of the average operating conditions. Once the size of the rectangular area has been determined, actual limits for the variances can be calculated.

Hence, we choose to set $y_0 = z_0$ because the sidescan sonar geometry is such that an angle of incidence of 45° points roughly to the middle of a one-sided cross-track profile (Condition 2 in Section 3.1). Moreover, a common standard deviation, $\tilde{\gamma}$, is assigned for the attitude rotations (Condition 4 in Section 3.1), so that Eqs. (55–56) are reduced to Eqs. (D1–D2) in Appendix D.

Ideally, we are looking for results that are valid regardless of the shape of the terrain in the area surveyed. In practice, we need to evaluate the reference slope variance, ζ^2, for a typical model of the seafloor. However, it will be shown that the choice of the seafloor model is not critical. In a first model, we just use a flat patch. The dimensions can be calculated from:

$$\rho_x^2 \approx \left[1 + \frac{\rho_y}{\Delta y}\frac{\tilde{\gamma}^2}{\tilde{\xi}^2}\right]\rho_y^2. \tag{59}$$

$$\rho_y \approx 1.9[\Delta x \Delta y\, z_0^2]^{1/4}\left[\frac{\tilde{\xi}}{\tilde{\zeta}}\right]^{1/2}\left[1 + \frac{\rho_y}{\Delta y}\frac{\tilde{\gamma}^2}{\tilde{\xi}^2}\right]^{-1/8} \tag{60}$$

(Appendix D-I.a).

The first equation is written in a way that emphasizes the order relation $\rho_x \geq \rho_y$. Eq (60) defines a fast converging process whose seed can be deduced from either of two limit cases: Whenever the noise in the elevation measurement is large enough, the factor in brackets that is present in both Eqs. (59) and (60) can be approximated by unity. This leads to the simple result:

$$\rho_x \approx \rho_y \approx 1.9[\Delta x \Delta y\, z_0^2]^{1/4}\left[\frac{\tilde{\xi}}{\tilde{\zeta}}\right]^{-1/2}, \tag{61}$$

whose condition of validity is found by replacing this value of ρ_y in the initial assumption:

$$\frac{\rho_y}{\Delta y}\frac{\tilde{\gamma}^2}{\tilde{\xi}^2} \approx 1.9\left[\frac{\Delta x\, z_0^2}{(\Delta y)^3}\right]^{1/4}\left[\frac{\tilde{\gamma}^4}{\tilde{\zeta}\tilde{\xi}^3}\right]^{1/2} \ll 1. \tag{62}$$

From a practical point of view, it is important to notice that if this condition is verified, the influence of the attitude angular movements is negligible to determine the size of the patch, hence solely defined by the noise remaining in the processed data ($\tilde{\xi}$). Another theoretical limit case applies if the orders of magnitude in Eq. (62) are reversed (Appendix D-I.b), yielding an alternative seed (Eq. D11) for the general iterative solution (Eq. 60).

As a second situation, the inverse problem is solved for a seafloor model whose across-track and along-track slopes lie, with a constant probability, between $-45°$ and 45° (consistent with Condition 3 of Section 3.1). Details are found in Appendix D-II. The results take now a form very similar to the previous case Eqs. (59–60):

$$\rho_x^2 \approx 1.1\left[1 + 1.3\frac{\rho_y}{\Delta y}\frac{\tilde{\gamma}^2}{\tilde{\xi}^2}\right]\rho_y^2, \tag{63}$$

$$\rho_y \approx 1.8[\Delta x \Delta y\, z_0^2]^{1/4}\left[\frac{\tilde{\xi}}{\tilde{\zeta}}\right]^{1/2}\left[1 + 1.3\frac{\rho_y}{\Delta y}\frac{\tilde{\gamma}^2}{\tilde{\xi}^2}\right]^{-1/8}, \tag{64}$$

with the same seeds (Eq. 61 or D11) as above. Consequently, numerical values derived from both seafloor models will be very close. This suggests that it is not important to use a more sophisticated seafloor model to answer our initial question.

3.3. Applications and numerical examples

We are looking now for numerical figures. First, the across-track step, Δy, is chosen consistently with the level of noise remaining in the processed elevation data, i.e.:

$$\Delta y \approx h\tilde{\xi}. \tag{65}$$

With a system such as SeaMARC II, the following numerical values are common:

$$\tilde{\alpha} \approx \tilde{\beta} \approx \tilde{\mu} \approx 1/100 \text{ rad}, \quad \tilde{\xi} \approx 1/20 \text{ rad},$$
$$z_0 = 3000\, m \quad \text{and} \quad \Delta x \approx 40\, m \tag{66}$$
$$(y_0 = z_0 \text{ and } \Delta y \approx 150 m).$$

Using these parameters, we are looking for the minimal size of a flat patch whose slopes can be

determined within an accuracy of 1/10 rad in both directions. In that case, one finds that the left side of Eq. (62) is about 0.17, so that the approximate result given in Eq. (61) applies:

$$\rho_x \approx \rho_y \approx 640\ m. \tag{67}$$

The standard deviation for the average altitude above the bottom (Eq. 57) lies around 18 m.

Assuming now that the noise in the elevation measurement is lower:

$$\tilde{\xi} \approx 1/30 \text{ rad} \qquad (\Delta y \approx 150\ m), \tag{68}$$

the condition given in Eq. (62) is no longer satisfied, and the general solution must be used (Eqs. 59–60), taking either Eq. (61) or Eq. (D11) to seed Eq. (18). In that case, one finds that the minimal size of the patch is:

$$\rho_x \gtrsim 530\ m \quad \text{and} \quad \rho_y \gtrsim 450\ m, \tag{69}$$

with the standard deviation for the average altitude above the bottom lying around 15 m.

These results give an indication on the size of the window that must be used to convolve SeaMARC II data in order to obtain a smooth, reliable bathymetry. On the other hand, they also provide information on the resolution of a bathymetric sidescan sonar system. For SeaMARC II, with parameters defined in Eq. (66), one cannot expect to obtain a reliable bathymetric representation of features whose surface extent is significantly smaller than the size given in Eq. (67). Values given in Eqs. (67, 69) are in agreement with the minimal size of the window that are used in practice to filter SeaMARC II data [8, 9]. In addition, rms differences between the bathymetry resulting from a nearly complete Sea Beam mapping of Fieberling Guyot (32.5°N–128°W), and SeaMARC II bathymetry collected over this Guyot were found to be less than 35 m [10]. Considering the difficult mapping geometry presented to the SeaMARC II system by a Guyot rising some 4000 m above the surrounding seafloor, and the uncertainties associated with the Sea Beam bathymetry taken as a reference, this result is compatible with the expected deviation calculated above in this section.

If filtering with a window of appropriate length is not performed, the accuracy of the representation is degraded. For example, using the solution of the direct problem (Eqs. 55–57), with the same parameters as above (Eq. 66), and scanning a flat, horizontal square patch of 300 m×300 m, the variance over the slopes in both directions is large ($\tilde{\zeta} \approx 0.45 \text{ rad} \approx 25°$), resulting in meaningless slope estimates.

Summary and Conclusions

A theoretical investigation about the spatial characteristics of seafloor representations obtained by means of a bathymetric sidescan sonar system has been presented. The effects of the platform's movements and of the specific polar form (range and elevation angles) with which such a system gathers data are emphasized.

First, formulas that allow to calculate the theoretical location of quasi punctual targets have been derived. The second order general solution (Eqs. 10–15) is given for reference and to calculate "exact" results, i.e. beyond realistic accuracy. Eqs. (17–19) apply when the platform does not drift. The more practical, first order solution which is common to both cases (with or without drift) is written in Eqs. (20–23). The specific influence of errors in each parameter on the uncertainty in target location is evaluated and discussed. This analysis applies for both bathymetry and sidescanned acoustic imagery of the seafloor.

In the next step, general expressions for the variance in the slopes and altitude estimates of a plane, rectangular patch of seafloor are derived, depending on the size and orientation of the seafloor patch, as well as its location with respect to the fish (Eqs. 55–58). This allows to solve the inverse problem which is central in this study. The solution of the inverse problem gives, in practice, an indication on the size of the window that must be used to filter noise out of the bathmetry. As a consequence, the solution also provides information about the actual horizontal resolution of the final isobath map.

We summarize here the recipe for calculating these lengths. If the condition given in Eq. (62) is verified, the solution is written in Eq. (61). Otherwise, the latter equation provides a seed for the fast converging recursive formula given in Eq. (60). The across-track length is then used in Eq. (59) for finding the along-track length.

For the sake of clarity, the derivation shown in this paper is performed by using the assumption that the angular movements of the fish (pitch, yaw, roll) have the same average amplitude. However, more specific solutions can be easily derived by following our method, starting from the solution of the direct problem (Eqs. 55–57).

The test mentioned previously (Eq. 62) underscores the critical effect of the uncertainty in elevation angle. In practice, the accuracy of across-track slope estimation depends mostly on this parameter (Eq. 58). In certain cases (Eq. 62) it may be also the main contribution to along-track errors in slope estimates and in average altitude, overshadowing uncertainties due to the attitude parameters. As a result, areas surveyed with low grazing angles are poorly represented. For example, this situation occurs with SeaMARC II for which the standard deviation of the elevation angle error can be as large as 1/20 rad. In any case, as expected, the bathymetry of a scarp when surveyed along-strike will be more accurate on the up-hill than on the down-hill side.

Acknowledgements

This work has been supported by the Office of Naval Research through grants N00014-90-J-1781 and N00014-91-J-1073. We thank Jo Griffith for the art work.

Appendices

A. Hypotheses

The following hypotheses are used in the derivation. They match normal operating conditions of sidescan sonar systems and therefore do not restrict the generality of the results. Ray bending has not been taken into account, but a) variations in travel time are handled as part of the error analysis (Section 2), and b) mislocation due to ray bending can be applied on top of the results of our analysis.

Hypothesis I:
With a sidescan sonar system, the beam pattern of the transducers is a fan that is narrow in the horizontal plane:

$$\theta_{3dB} \ll 1, \qquad (\text{e.g. } \theta_{3dB} \approx 1/20 \text{ rad}) \tag{A1}$$

The speed of the survey is chosen so that the distance traveled between transmit (P) and receive (Q) is smaller than the along-track dimension of the footprint of the beam on the seafloor to ensure 100% coverage along-track. Hence:

$$PQ/JM \lesssim \theta_{3dB} \tag{A2}$$

As a consequence of Eq. (A1), the following conditions are always met, even with a deep-towed system:

$$PQ \ll JM \Rightarrow i \ll s. \tag{A3}$$

Hypothesis II:
Again, to ensure proper operating conditions, the fish which carries the antenna is designed to provide enough stability so that transmit and receive beam patterns overlap sufficiently. This requires that the differences $(\alpha_T - \alpha_R)$ and $(\beta_T - \beta_R)$ follow a condition similar to Eq. (A2):

$$|\alpha_T - \alpha_R| \lesssim \theta_{3dB} \quad \text{and} \quad |\beta_T - \beta_R| \lesssim \theta_{3dB}, \tag{A4}$$

so that, from Eq. (A1), there is also:

$$|\alpha_T - \alpha_R| \ll 1 \quad \text{and} \quad |\beta_T - \beta_R| \ll 1. \tag{A5}$$

Hypothesis III:
The fish is towed along the x-axis, so that it is not restrictive to assume that the lateral variations j and k remain much smaller than the along-track progression, i:

$$j/i \ll 1 \quad \text{and} \quad k/i \ll 1. \tag{A6}$$

Eq. (A6) is usually verified as long as α_T, β_T, α_R and $\beta_R \ll 1$. However, if one of these angular conditions of attitude is not true, and because of the previous condition (Eq. A5), Eq. (A6) may still be verified if the fish is drifting in the corresponding plane. For example, with $\alpha_T \approx \alpha_R \approx 10°$ ($|\alpha_T - \alpha_R| \ll 1$), and a strong lateral drift current (same value, i.e. around 10°), the variations in true heading remain small and still yield $j/i \ll 1$.

Hypothesis IV:
Finally, attitudes angles, as well as elevation error ξ, must remain small enough to permit developments of trigonometric functions up to the second order ($\sin\gamma \approx \tan\gamma \approx \gamma$ and $\cos\gamma \approx 1 - \gamma^2/2$). This is true as long as:

$$\alpha_T^2, \beta_T^2, \alpha_R^2, \beta_R^2, \mu^2, \xi^2 \ll 1. \tag{A7}$$

In finding the location of a target M as defined in Section 1.1, a direct computation is cumbersome and the level of approximation to apply is critical in order to derive pertinent results. With s as a reference length, the orders of magnitude are ranked to indicate which contributions will be omitted:

- $(\alpha_T, \alpha_R, \beta_R, \beta_T, \mu, \xi)s$ and i are considered first order lengths;
- $(\alpha_T, \alpha_R, \beta_R, \beta_T, \mu, \xi)i$, (any angle product $\gamma\nu)s$, j and k are second order terms.

The developments will carried up to the second order, i.e. terms like $(\alpha_T\mu\alpha_R s)$, $(\alpha_T\alpha_R i)$ or (αj) will be discarded. Hypothesies I through IV being verified, rather large attitudes angles are still possible. For example, with a roll amplitude μ of up to 10°, the accuracy over z will remain better than 0.1% (third order component in the development of $\sin\mu$ is $\mu^3/6 = 8.9\ 10^{-4}$).

B. Steps in the derivation

Notation: Following Eq. (2), let X, Y, Z denote the coordinates of vector $\overrightarrow{JM}$ that emphasize the target location with respect to the fish's position at mid travel between transmit and receive:

$$\overrightarrow{JM} = (X, Y, Z) = \overrightarrow{OM} - \overrightarrow{OP} - \overrightarrow{PQ}/2, \tag{B1}$$

in which O is the origin of the cartesian coordinate system, i.e.:

$$X = x - l - i/2, \quad Y = y - m - j/2, \quad Z = z - n - k/2. \tag{B2}$$

Using matrix notations to describe rotations, roll pitch and yaw

are given respectively by the following matrices:

$$M_x(\mu) = \begin{bmatrix} 1 & 0 & 0 \\ 0 & \cos\mu & -\sin\mu \\ 0 & \sin\mu & \cos\mu \end{bmatrix},$$

$$M_y(\beta) = \begin{bmatrix} \cos\beta & 0 & \sin\beta \\ 0 & 1 & 0 \\ -\sin\beta & 0 & \cos\beta \end{bmatrix}, \tag{B3}$$

$$M_x(\mu) = \begin{bmatrix} \cos\alpha & -\sin\alpha & 0 \\ \sin\alpha & \cos\alpha & 0 \\ 0 & 0 & 1 \end{bmatrix},$$

SECTION B-I

The elevation angle ψ from the sonar to the target is defined as the angle by which the vertical plane containing $\vec{R}$ must be rotated around this vector to include the target. In order to express the first condition listed in Section 1.1 (Eq. 6), we denote $\vec{A}$ the unit vector such the $(Q, \vec{A})$ defines this tilted plane Π containing the target M ($Q \in \Pi$, $\vec{A} \perp \Pi$. Using matrix notation, $\vec{A}$ is expressed by:

$$\vec{A} = M_z(\alpha_R)M_y(\beta_R)M_x(\psi)\begin{bmatrix} 0 \\ 1 \\ 0 \end{bmatrix}.$$

$$= M_z(\alpha_R)M_y(\beta_R)\begin{bmatrix} 0 \\ \cos\psi \\ \sin\psi \end{bmatrix}. \tag{B4}$$

Note that in Figure 1b, $(\vec{R}, \vec{y}', \vec{z}')$ is the reference frame of the fish corrected for roll, so $\vec{y}'$ is the horizontal unit vector perpendicular to $\vec{R}$ and $\vec{z}$, and $\vec{z}'$ forms an orthonormal base with $\vec{R}$ and $\vec{y}'$. Using this reference frame, Eq. (B4) is simply written:

$$\vec{A} = \vec{y}'\cos\psi + \vec{z}'\sin\psi. \tag{B5}$$

Taking J as the origin of coordinates (Eq. 2), any point M in the plane (Eq. 6) satisfies:

$$\overrightarrow{JM} \cdot \vec{A} = \tfrac{1}{2}\overrightarrow{PQ} \cdot \vec{A}. \tag{B6}$$

SECTION B-II

The second condition of Section 1.1 defines the ellipsoid where M lies at constant range from P to Q (Eq. 7). To find an approximation of this surface in the athwartship sector, the law of cosines is applied to the triangle PQM, yielding:

$$PM^2 - QM^2 = 2\overrightarrow{PQ} \cdot \overrightarrow{JM}. \tag{B7}$$

Expanding the left side into a sum and difference product and using Eqs. (7) and (B1), this equation becomes:

$$\overrightarrow{PQ} \cdot \overrightarrow{JM} = s[|\overrightarrow{JM} + \overrightarrow{PQ}/2| - |\overrightarrow{JM} - \overrightarrow{PQ}/2|]. \tag{B8}$$

As shown in Hypothesis I (Eqs. AI–3), the distance PQ between the focus points is much smaller than the average radius s. Consequently, if $|\overrightarrow{JM}|$ is factored out on the right side of Eq. (B8), the remainder can be expanded in a Taylor series, keeping terms up to the third order in (PQ/JM):

$$\overrightarrow{PQ} \cdot \overrightarrow{JM} = sJM\left[\frac{\overrightarrow{PQ} \cdot \overrightarrow{JM}}{JM^2} - \frac{PQ^2(\overrightarrow{PQ} \cdot \overrightarrow{JM})}{8JM^4} + \frac{(\overrightarrow{PQ} \cdot \overrightarrow{JM})^3}{8JM^6}\right]. \tag{B9}$$

Under normal operating conditions, for any given ping, the cross-track profile of the bottom measured by the sidescan sonar lies in a plane that is approximately perpendicular to the direction of motion $\overrightarrow{PQ}$. Hence, $\overrightarrow{PQ} \cdot \overrightarrow{JM}$ is at least one order of magnitude smaller than the scalar product $|\overrightarrow{PQ}||\overrightarrow{JM}|$, so that the last term on the right side of Eq. (B9) is actually of fourth order and can be neglected, yielding after simplification:

$$JM = s\left[1 - \frac{PQ^2}{8JM^2}\right] \tag{B10}$$

Squaring both sides of this equation and solving for JM^2 up to the third order yields the equation of the inner sphere tangent to the ellipsoid ($JM^2 = s^2 - (PQ/2)^2$, Eq. (8)).

SECTION B-III

Considering Condition 3 in Section 1.1, the plane $(\Pi_T) = (P, \vec{T})$, represents the across-track area of maximal insonification in the farfield of the transmitter (Figure 2). Likewise, the corresponding plane at reception is $(\Pi_R) = (Q, \vec{R})$. In the ideal case where the sonar experiences no pitch, or yaw, these two planes are parallel. In cases where there is pitch or yaw, they intersect along a line, so that for any point I along that line:

$$\overrightarrow{IP} \cdot \vec{T} = 0. \tag{B11}$$

$$\overrightarrow{IQ} \cdot \vec{R} = 0. \tag{B12}$$

Following Hypothesis Π (Eqs. A4–5), the dihedral angle formed by planes $(P, \vec{T})$ and $(Q, \vec{R})$ is very small and remains within the same range as the angle measured at the half-power point of the one-way beam patterns (receive and transmit beam patterns are supposed to be identical). Hence with Hypothesis I (Eqs. A1–3), it is reasonable to approximate the locus of the maxima of the product of the farfield beam patterns by the plane (Π_M) bisecting the dihedral angle. Consequently, for any point M in the bisecting plane,

$$\overrightarrow{IM} \cdot (\vec{R} + \vec{T}) = 0. \tag{B13}$$

Using Eqs. (2, B11–12), I is eliminated from Eq. (B13), yielding:

$$(\vec{R} + \vec{T}) \cdot \overrightarrow{JM} = (\vec{R} - \vec{T}) \cdot \overrightarrow{PQ}/2, \tag{B14}$$

which remains valid when the transmit and receive planes do not intersect, i.e. $\vec{R} = \vec{T}$. The magnitude of the right side of this equation is of third order, so it is discarded when handling the analytical calculation ($(\vec{R} + \vec{T}) \cdot \overrightarrow{JM} = 0$, Eq. (9)).

SECTION B-IV

Solving the set of Eqs. (B6, 8–9) is conveniently performed by first partially solving the two linear Eqs. (B6) and (9). Both equations are rewritten here using the notation introduced in

Eq. (B2) and omitting part of the terms beyond the second order, but for clarity not always expanding $\tan\psi$:

$$X[\alpha_R - \beta_R\tan\psi] - Y[1 - \tfrac{1}{2}\alpha_R^2 + \beta_R\alpha_R\tan\phi] = Z\left[\tan\psi - \beta_R^2\frac{\tan\phi}{2}\right] - \tfrac{1}{2}[i(\beta_R\tan\phi - \alpha_R) + j + k\tan\phi], \tag{B15}$$

and

$$X[2 - \tfrac{1}{2}(\alpha_T^2 + \alpha_R^2 + \beta_T^2 + \beta_R^2)] + Y(\alpha_T + \alpha_R) = Z(\beta_R + \beta_T). \tag{B16}$$

One obtains the partial solution for this system as a function of Z:

$$X = \tfrac{1}{2}Z[(\alpha_T + \alpha_R)\tan\psi + (\beta_T + \beta_R)], \tag{B17}$$

and

$$Y = Z\left[-\tan\psi + \alpha_R\beta_R\frac{1}{2\cos^2\phi} + \tfrac{1}{2}(\alpha_T\tan\phi + \beta_T)(\alpha_R - \beta_R\tan\phi)\right] + \tfrac{1}{2}[i(\beta_R\tan\phi - \alpha_R) + j + k\tan\phi]. \tag{B18}$$

Combining the partial solution with the equation of the sphere (Eq. 8) yields the following quadratic equation in Z (reduced to the second order).

$$Z^2\{1 + \tfrac{1}{4}[(\alpha_T + \alpha_R)\sin\phi + (\beta_R + \beta_T)\cos\phi]^2 - \tan\phi[\alpha_R\beta_R + (\alpha_T\sin\phi + \beta_T\cos\phi)(\alpha_R\cos\phi - \beta_R\sin\phi)]\} - Z\sin\phi[i(\beta_R\sin\phi - \alpha_R\cos\phi) + j\cos\phi + k\sin\phi] + i^2\frac{\cos^2\phi}{4} - s^2\cos^2\psi = 0. \tag{B19}$$

As previously, trigonometric expressions of the elevation ψ stand for their development given in Eqs. (10–11). The solution of Eq. (B19) is calculated up to the second order:

$$Z = s\cos\psi - \tfrac{1}{2}s\left\{\beta_R[(\alpha_T - \alpha_R)\sin\phi + \beta_T\cos\phi)] + \frac{\cos\phi}{4}[(\alpha_T - \alpha_R)\sin\phi + (\beta_T - \beta_R)\cos\phi]^2\right\} - \frac{i^2}{8s}\cos\phi + \frac{\sin\phi}{2}[i(\beta_R\sin\phi - \alpha_R\cos\phi) + j\cos\phi + k\sin\phi]. \tag{B20}$$

Then, replacing Z in Eqs. (B17–18) gives respectively the along-track and across-track coordinates:

$$X = \tfrac{1}{2}s\{(\alpha_T + \alpha_R)\sin\phi + (\beta_T + \beta_R)\cos\phi + (\mu + \xi)[(\alpha_T + \alpha_R)\cos\phi - (\beta_T + \beta_R)\sin\phi]\}, \tag{B21}$$

$$Y = -s\sin\psi + \frac{s}{2}\left\{\alpha_R[\alpha_T\sin\phi + (\beta_T + \beta_R)\cos\phi] + \frac{\sin\phi}{4}[(\alpha_T - \alpha_R)\sin\phi + (\beta_T - \beta_R)\cos\phi]^2\right\} + \frac{i^2}{8s}\sin\phi + \frac{\cos\phi}{2}[i(\beta_R\sin\phi - \alpha_R\cos\phi) + j\cos\phi + k\sin\phi]. \tag{B22}$$

Eqs. (B20–22), in conjunction with Eq. (B2), give all the terms that should be taken into account in the worst cases. However, by adding some realistic assumptions, a variety of results can be derived from this set of equations. First, the along-track dimension of the beam footprint is commensurate with $s\theta_{3dB}$, i.e. a first order quantity (Eq. A2). Hence, second order terms in Eq. (B21) are much smaller and can be disregarded in the determination of x. In addition, as mentioned above, the along-track component of $\overrightarrow{PQ}$ (i.e. i) is always much smaller than the range s. Although i/s is considered and kept as a first order quantity, the ratio $i^2/(8s^2)$ is always much smaller than other second order terms in Eqs. (B20, B22) and can be neglected. On the other hand, large variations of pitch or yaw are unlikely to occur within the time interval between pulse transmission and seafloor backscatter signal reception. For instance, yaw at transmit can be as large as $\alpha_T \approx 1/5$ rad, as would occur in a strong lateral current or during a course change, although the rate of change of yaw is slow enough so that the difference in yaw between transmit and receive remains smaller than $|\alpha_T - \alpha_R| \lesssim (1/50$ rad. As a result, yaw and pitch values can be substituted by their average (E. 15), and the second order terms involving the variations of these angles can be disregarded. Applying these approximations to Eqs. (B20–B22) leads finally to the set of simplified relations given in the text (Eqs. 12–14) that is used subsequently.

C. Variance calculations

First, we express the solution of the least squares problem in Eqs. (47–48). For a regular, rectangular grid as defined in Eqs. (44–45), the general solution is:

$$\Delta x\tan\zeta_x = \frac{-3}{L(L+1)(2L+1)(2W+1)}\sum_p\left[p\sum_q z_{p,q}\right], \tag{C1}$$

$$\Delta y\tan\zeta_y = \frac{3}{W(W+1)(2W+1)(2L+1)}\sum_q\left[q\sum_p z_{p,q}\right], \tag{C2}$$

and

$$h = \frac{1}{(2L+1)(2W+1)}\sum_p\sum_q z_{p,q}. \tag{C3}$$

The samples $z_{p,q}$ are given in Eq. (46), in which terms δx, δy and δz are derived from Eqs. (36–38). Recalling that the problem is restricted to small-scale fluctuations, the transmit point P can be reset to the origin of the coordinate system ($l = m = n = 0$). Moreover, in calculating δx and δy, z is replaced by its value at the reference points (x_p, y_q). The along-track translations due to yaw (α) and pitch (β) are then:

$$\delta x \approx \beta_p(z_0 - p\Delta x\tan\theta_x + q\Delta y\tan\theta_y) - \alpha_p(y_0 + q\Delta y). \tag{C4}$$

Similarly, the across-track translations due to roll (μ) plus the

noise due to the bathymetry processing (ξ) are:

$$\delta y = -(\mu_p + \xi_{p,q})(z_0 - p\Delta x \tan\theta_x + q\Delta y \tan\theta_y), \quad \text{(C5)}$$

and the vertical variations due to the same causes are

$$\delta z \approx (\mu_p + \xi_{p,q})(y_0 + q\Delta y). \quad \text{(C6)}$$

Replacing these expressions in Eq. (46) yields:

$$\begin{aligned} z_{p,q} = z_0 &- p\Delta x \tan\theta_x + q\Delta y \tan\theta_y \\ &- [\alpha_p(y_0 + q\Delta y) \\ &+ \beta_p(z_0 - p\Delta x \tan\theta_x + q\Delta y \tan\theta_y)]\tan\theta_x \\ &- (\mu_p + \xi_{p,q})\left[y_0 + (z_0 - p\Delta x \tan\theta_x)\tan\theta_y \right. \\ &\left. + q\Delta y \frac{1}{\cos^2\theta_y}\right]. \end{aligned} \quad \text{(C7)}$$

As parameters α_p, β_p, μ_p, and $\xi_{p,q}$ have zero mean, the slopes and the depth, that are solutions of Eqs. (C1–C3), have expected values:

$$E[h] = z_0, \quad E[\zeta_x] = \theta_x, \quad E[\zeta_y] = \theta_y. \quad \text{(C8)}$$

However, we are interested in the variances over these results. To this end, it is necessary to derive first the expression of their particular occurrence. Hence, developing Eqs. (C1–C3) yields:

$$\begin{aligned} \tan\zeta_x = \tan\theta_x &- \frac{3}{L(L+1)(2L+1)\Delta x} \\ &\times \sum_p p\{[\alpha_p y_0 - \beta_p(z_0 - p\Delta x \tan\theta_x)]\tan\theta_x \\ &\quad - \mu_p[y_0 + (z_0 - p\Delta x \tan\theta_x)\tan\theta_y]\} \\ &+ \frac{3}{L(L+1)(2L+1)(2W+1)\Delta x} \\ &\times \sum_p \sum_q p\left\{y_0 + (z_0 - p\Delta x \tan\theta_x)\tan\theta_y \right. \\ &\left. + q\Delta y \frac{1}{\cos^2\theta_y}\right\}\xi_{p,q}, \end{aligned} \quad \text{(C9)}$$

$$\begin{aligned} \tan\zeta_y = \tan\theta_y &+ \frac{1}{2L+1}\sum_p\left[(\alpha_p - \beta_p\tan\theta_y)\tan\theta_x - \mu_p\frac{1}{\cos^2\theta_y}\right] \\ &- \frac{3}{W(W+1)(2W+1)(2L+1)\Delta y} \\ &\times \sum_p \sum_q q\left[y_0 + (z_0 - p\Delta x \tan\theta_x)\tan\theta_y \right. \\ &\left. + q\Delta y \frac{1}{\cos^2\theta_y}\right]\xi_{p,q}, \end{aligned} \quad \text{(C10)}$$

and

$$\begin{aligned} h = z_0 &+ \frac{1}{2L+1}\sum_p\{[\alpha_p y_0 - \beta_p(z_0 - p\Delta x \tan\theta_x)]\tan\theta_x \\ &\quad - \mu_p[y_0 + (z_0 - p\Delta x \tan\theta_x)\tan\theta_y]\} \\ &- \frac{1}{(2L+1)(2W+1)}\sum_p\sum_q\left\{y_0 + (z_0 - p\Delta x \tan\theta_x)\tan\theta_y \right. \\ &\left. + q\Delta y \frac{1}{\cos^2\theta_y}\right\}\xi_{p,q}. \end{aligned} \quad \text{(C11)}$$

Using the linearity of the variances for independant Gaussian variables, one deduces the variance of the offset as given in Eq. (C11):

$$\begin{aligned} \tilde{h}^2 = &\frac{1}{2L+1}\left\{\left[\tilde{\alpha}^2 y_0^2 + \tilde{\beta}^2\left[z_0^2 + \frac{L(L+1)}{3}(\Delta x)^2\tan^2\theta_y\right]\right]\tan^2\theta_x \right. \\ &+ \tilde{\mu}^2\left[(y_0 + z_0\tan\theta_y)^2 + \frac{L(L+1)}{3}(\Delta x)^2\tan^2\theta_x\tan^2\theta_y\right] \\ &+ \frac{1}{2W+1}\tilde{\xi}^2\left[(y_0 + z_0\tan\theta_y)^2 \right. \\ &\quad + \frac{L(L+1)}{3}(\Delta x)^2\tan^2\theta_x\tan^2\theta_y \\ &\left.\left. \quad + \frac{W(W+1)}{3}(\Delta y)^2\frac{1}{\cos^4\theta_y}\right]\right\}. \end{aligned} \quad \text{(C12)}$$

In looking for relatively small standard deviations, $\tilde{\zeta}$, over the slope angles, the following approximate relation with deviations in tangents, $\tilde{\tau}$, is used:

$$\tilde{\zeta} \approx \tilde{\tau}\cos^2\theta, \quad \text{(C13)}$$

and, one deduces from Eqs. (C9–C10):

$$\begin{aligned} \tilde{\zeta}_x^2 = &\frac{3\cos^2\theta_x}{L(L+1)(2L+1)(\Delta x)^2} \\ &\times\left\{\left[\tilde{\alpha}^2 y_0^2 + \tilde{\beta}^2\left[z_0^2 + \frac{3L^2+3L-1}{5}(\Delta x)^2\tan^2\theta_x\right]\right]\sin^2\theta_x \right. \\ &\quad + \tilde{\mu}^2\left[(y_0 + z_0\tan\theta_y)^2\cos^2\theta_x \right. \\ &\left.\left. \quad + \frac{3L^2+3L-1}{5}(\Delta x)^2\tan^2\theta_y\sin^2\theta_x\right]\right. \\ &+ \frac{1}{2W+1}\tilde{\xi}^2\left[(y_0 + z_0\tan\theta_y)^2\cos^2\theta_x \right. \\ &\quad + \frac{3L^2+3L-1}{5}(\Delta x)^2\tan^2\theta_y\sin^2\theta_x \\ &\left.\left. \quad + \frac{W(W+1)}{3}(\Delta y)^2\frac{\cos^2\theta_x}{\cos^4\theta_y}\right]\right\}, \end{aligned} \quad \text{(C14)}$$

and

$$\begin{aligned} \tilde{\zeta}_y^2 = &\frac{1}{2L+1}\left\{(\tilde{\alpha}^2\cos^2\theta_y + \tilde{\beta}^2\sin^2\theta_y)\tan^2\theta_x\cos^2\theta_y + \tilde{\mu}^2 \right. \\ &\quad + \frac{1}{W(W+1)(2W+1)(\Delta y)^2} \\ &\quad \times\tilde{\xi}^2\left[3(y_0\cos\theta_y + z_0\sin\theta_y)^2\cos^2\theta_y \right. \\ &\quad + L(L+1)(\Delta x)^2\tan^2\theta_x\sin^2\theta_y\cos^2\theta_y \\ &\left.\left. \quad + \frac{3(3W^2+3W-1)}{5}(\Delta y)^2\right]\right\}, \end{aligned} \quad \text{(C15)}$$

Eqs. (C12, C14–C15) are wwritten for reference purpose, and to allow checking intermediate calculations and further approximations. Although seemingly busy, these equations can be easily simplified by comparing the order of magnitude of each term,

deduced from some basic remarks which listed in the main text. Using these conditions, Eq. (C14) can be approximated by:

$$\tilde{\zeta}_x^2 \approx 12\cos^2\theta_x \frac{\Delta x}{\rho_x^3}\frac{(L+1/2)^2}{L(L+1)} \times\left[(\tilde{\alpha}^2 y_0^2+\tilde{\beta}^2 z_0^2)\sin^2\theta_x + \left(\tilde{\mu}^2+\frac{1}{2W+1}\tilde{\xi}^2\right)(y_0+z_0\tan\theta_y)^2\cos^2\theta_x\right], \tag{C16}$$

Eq. (C15) gives:

$$\tilde{\zeta}_y^2 \approx \frac{1}{2L+1}\left[(\tilde{\alpha}^2\cos^2\theta_y+\tilde{\beta}^2\sin^2\theta_y)\tan^2\theta_x\cos^2\theta_y+\tilde{\mu}^2 + \tilde{\xi}^2\frac{12\Delta y}{\rho_y^3}\frac{(W+1/2)^2}{W(W+1)} \times(y_0\cos\theta_y+z_0\sin\theta_y)^2\cos^2\theta_y\right], \tag{C17}$$

whereas Eq. (C12) is reduced to:

$$\tilde{h} \approx \frac{1}{2L+1}\left[(\tilde{\alpha}^2 y_0^2+\tilde{\beta}^2 z_0^2)\tan^2\theta_x + \left(\tilde{\mu}^2+\frac{1}{2W+1}\tilde{\xi}^2\right)(y_0+z_0\tan\theta_y)^2\right]. \tag{C18}$$

D. Inverse problem

To find a solution to the inverse problem stated at the beginning of Section 3.2 one calculates first the variances in slopes associated with the patch of seafloor centered at $y_0 = z_0$, and with $\tilde{\delta} \approx \tilde{\beta} \approx \tilde{\mu} \approx \tilde{\gamma}$. Eqs. (55–56) can be rewritten as:

$$\tilde{\zeta}_x^2 \approx 12\cos^2\theta_x\frac{\Delta x\, z_0^2}{\rho_x^3} \times\left[2\sin^2\theta_x\tilde{\gamma}^2+(1+\tan\theta_y)^2\cos^2\theta_x\left(\tilde{\gamma}^2+\tilde{\xi}^2\frac{\Delta y}{\rho_y}\right)\right], \tag{D1}$$

$$\tilde{\zeta}_y^2 \approx \frac{\Delta x}{\rho_x}\left[(1+\tan^2\theta_x\cos^2\theta_y)\tilde{\gamma}^2 + 12(1+\sin 2\theta_y)\cos^2\theta_y\frac{\Delta y\, z_0^2}{\rho_y^3}\tilde{\xi}^2\right], \tag{D2}$$

D-I. Flat patch

Section D-I.1.

With $\theta_x = \theta_y = 0$, Eqs. (D1–D2) yield:

$$\tilde{\zeta}_x^2 \approx 12\frac{\Delta x\, z_0^2}{\rho_x^3}\left[\tilde{\gamma}^2+\frac{\Delta y}{\rho_y}\tilde{\xi}^2\right], \tag{D3}$$

$$\tilde{\zeta}_y^2 \approx \frac{\Delta x}{\rho_x}\left[\tilde{\gamma}^2+12\frac{\Delta y\, z_0^2}{\rho_y^3}\tilde{\xi}^2\right]. \tag{D4}$$

There is no explicit analytical solution (ρ_x, ρ_y) for this system. However, the implicit form as written in the following provides a numerical solution:

$$\rho_x^2 \approx \left[1+\frac{\rho_y}{\Delta y}\frac{\tilde{\gamma}^2}{\tilde{\xi}^2}\right]\left[1+\frac{\rho_y^3\tilde{\gamma}^2}{12\Delta y\, z_0^2\tilde{\xi}^2}\right]^{-1}\rho_y^2.$$

$$\rho_y = [12\Delta x\Delta y\, z_0^2]^{1/4}\left[\frac{\tilde{\xi}}{\tilde{\zeta}}\right]^{1/2}\left[1+\frac{\rho_y}{\Delta y}\frac{\tilde{\gamma}^2}{\tilde{\xi}^2}\right]^{-1/8} \times\left[1+\frac{\rho_y^3\tilde{\gamma}^2}{12\Delta y\, z_0^2\tilde{\xi}^2}\right]^{3/8}. \tag{D6}$$

The latter equation contains the only unknown ρ_y. It is a fast converging iterative formula. Equating the right sides of Eqs. (D3–D4) and recalling that we are only interested in a solution that verifies $\rho_x \lesssim z_0$ (Eq. 49), one sees that the second term in Eq. (D4) is at least 11 times larger than the first one, i.e.:

$$\frac{\rho_y^3\tilde{\gamma}^2}{12\Delta y\, z_0^2\tilde{\xi}^2} \ll 1. \tag{D7}$$

Incidentally, looking back at the direct problem, Eq. (D7) shows that only the noise term $(\tilde{\xi})$ is perminent in finding the across-track slope, hence it is generally possible to proceed with the reduction from Eq. (56) to Eq. (58).

It follows from Eq. (D7) that the right brackets in Eqs. (D5–D6) can be neglected, yielding Eqs. (59–60) in the text. Then, from Eq. (60), one calculates the slope of the right side of this iterative formula, seen as a function of ρ_y:

$$|\rho_y'| \approx \frac{1}{8}\frac{\rho_y}{\Delta y}\frac{\tilde{\gamma}^2}{\tilde{\xi}^2}\left[1+\frac{\rho_y}{\Delta y}\frac{\tilde{\gamma}^2}{\tilde{\xi}^2}\right]^{-1} < \frac{1}{8}. \tag{D8}$$

As this slope is small compared to unity, the convergence of the process is fast, and a single step is usually sufficient to obtain a correct figure.

Section D-I.2.

Two approximate solutions can be derived from Eqs. (59–60). The situation which is the more likely to be encountered in actual design, is presented in the text (Eqs. 61–62). The other case occurs if the condition written by reversing the order of magnitude in Eq. (62) is true, i.e.:

$$\frac{\rho_y}{\Delta y}\frac{\tilde{\gamma}^2}{\tilde{\xi}^2} \gg 1, \tag{D9}$$

It implies for instance that the noise in the elevation measurements $(\tilde{\xi})$ is not larger than the attitude angular variations (Eq. (49) being verified). With Eq. (D9), Eqs. (59–60) yield:

$$\rho_x = \left[12\Delta x\, z_0^2\frac{\tilde{\gamma}^2}{\tilde{\xi}^2}\right]^{1/3} \tag{D10}$$

and

$$\rho_y = \left[\Delta y\rho_x^2\frac{\tilde{\xi}^2}{\tilde{\gamma}^2}\right]^{1/3} \approx 1.7\left[(\Delta x)^2(\Delta y)^3 z_0^4\frac{\tilde{\xi}^6}{\tilde{\gamma}^2\tilde{\zeta}^4}\right]^{1/9}. \tag{D11}$$

This value for ρ_y can be used as an alternative seed in the iterative solution (Eq. 60) that applies in the more general case.

Section D-II. Model with uniform slope distribution

Integrating Eqs. (D1–D2) over θ_x and θ_y in the interval $[-45°, 45°]^2$ yields, respectively:

$$\tilde{\zeta}_x^2 \approx 12 \frac{\Delta x\, z_0^2}{\rho_x^3}\left[1.13\tilde{y}^2 + 0.88\frac{\Delta y}{\rho_y}\tilde{\xi}^2\right], \tag{D12}$$

$$\tilde{\zeta}_y^2 \approx \frac{\Delta x}{\rho_x}\left[1.14\tilde{y}^2 + 9.8\frac{\Delta y\, z_0^2}{\rho_y^3}\tilde{\xi}^2\right], \tag{D13}$$

which is very similar to the previous system (Eqs. D3–D4), yielding finally the system of Eqs. (63–64) in the text. If Eq. (62) is verified, the following approximate solution applies:

$$\rho_x \approx \rho_y = 1.8[\Delta x\, \Delta y\, z_0^2]^{1/4}\left[\frac{\tilde{\xi}}{\tilde{\zeta}}\right]^{1/2}, \tag{D14}$$

which is very close to Eq. (61).

If the orders of magnitude in Eq. (62) are reversed, the approximate solution takes the form:

$$\rho_x \approx 1.0\left[12\Delta x\, z_0^2 \frac{\tilde{y}^2}{\tilde{\zeta}^2}\right]^{1/3} \tag{D15}$$

and

$$\begin{aligned}\rho_y &\approx 0.9\left[\Delta y\, \rho_x^2 \frac{\tilde{\xi}^2}{\tilde{y}^2}\right]^{1/3} \\ &\approx 1.6\left[(\Delta x)^2(\Delta y)^3 z_0^4 \frac{\tilde{\xi}^6}{\tilde{y}^2\tilde{\zeta}^4}\right]^{1/9},\end{aligned} \tag{D16}$$

which is also very close to Eqs. (D10–D11).

References

1. de Moustier, C., 1988, State of the Art in Swath Bathymetry Survey Systems, *Int. Hyd. Review* **65**, 25–54.
2. de Moustier, C., 1993, Signal Processing for Swath Bathymetry and Concurrent Seafloor Acoustic Imaging, in: Moura & Lourtie (eds.), *Acoustic Signal Processing for Ocean Exploration,* NATO ASI, Kluwer, pp. 329–354.
3. Blackinton, J. G., 1986, Bathymetric Mapping with SeaMARC II: An Elevation Angle Measuring Side-Scan Sonar System, Ph.D. Dissertation, Hawaii Inst. of Geophys., Univ. of Hawaii, Manoa.
4. Matsumoto, H., Characteristics of SeaMARC II Phase Data, *IEEE J. Oceanic Eng.* **15**, 350–360.
5. Masnadi-Shirazi, M. A., de Moustier, C., Cervenka, P., and Zisk, S. H., 1992, Differential Phase Estimation with the SeaMARC II Bathymetric Sidescan Sonar System, *IEEE J. Oceanic Eng.* **17**, 239–251.
6. Blackinton , J. G., 1991, Bathymetric Resolution, Precision and Accuracy Considerations for Swath Bathymetry Mapping Sonar Systems, in: *Proc. IEEE Oceans '91,* Vol. 1, pp. 550–557.
7. Cobra, D. T., 1991, Estimation of Geometric Distortions in Side-Scan Images, *Proc. IEEE OES Oceans '91 Conf.*
8 Cervenka, P., de Moustier, C., and Lonsdale, P. F., 1990, Pixel Relocation in SeaMARC II Sidescan Sonar Images Based on Gridded Sea Beam Bathymetry, *Eos Transactions, American Geophysical Union* **71**, 1407–1408.
9. Cervenka, P., de Moustier, C., and Lonsdale, P. F., 1991, Corrections on SeaMARC II Sidescan Sonar Bathymetry, *Eos Trans. Am. Geophys. Un.* **72**, 249.
10. Cervenka, P., de Moustier, C., and Lonsdale, P. F., 1994, Geometric Corrections on Sidescan Sonar Images Based on Bathymetry. Application with SeaMARC II and Sea Beam Data, *Marine Geophys. Res.* (in press).